

A Basinwide Estimate of Vertical Mixing in the Upper Pycnocline: Spreading of Bomb Tritium in the North Pacific Ocean

DAN E. KELLEY

Department of Oceanography, Dalhousie University, Halifax, Nova Scotia, Canada

KIM A. VAN SCOY

Department of Atmospheric and Oceanic Science, University of Wisconsin—Madison, Madison, Wisconsin

(Manuscript received 3 October 1997, in final form 7 August 1998)

ABSTRACT

The vertical diffusivity K_v in the upper half-kilometer of the North Pacific subtropical pycnocline is estimated from observations of the spreading rate of anthropogenic tritium. The calculation is based on approximately 300 ocean tritium profiles made since tritium was introduced to the atmosphere via bomb testing in the 1960s. The data coverage does not permit detailed mapping of tritium penetration, especially in the sparsely sampled western Pacific. For this reason, and to minimize advective effects, the spreading rate is averaged within the closed streamlines of the subtropical gyre spanning $\sim 5^\circ\text{N}$ to $\sim 40^\circ\text{N}$. The result, $K_v = (1.5 \pm 0.7) \times 10^{-5} \text{ m}^2 \text{ s}^{-1}$, is consistent with inferences from microstructure and purposefully released tracer measurements in the North Atlantic, confirming that the spatially averaged rate of mixing in the upper pycnocline is substantially lower than the canonical Munk estimate for the lower pycnocline.

1. Introduction

Accounting for the effects of vertical mixing in large-scale ocean models requires parameterization because the spatial and temporal scales of mixing are too small to resolve directly. A common parameterization employs a nonisotropic analogy to molecular diffusion, with the diffusivity being divided into components, K_H and K_v , representing downgradient fluxes along and across geopotential surfaces, respectively.

Here we focus on vertical mixing in the upper pycnocline of subtropical gyres, near the level of the “mode” waters of the ventilated pycnocline (McCartney 1982; Luyten et al. 1983; Talley 1985; Woods and Barkmann 1986). The value of K_v in this zone may be important not just locally, but at the global scale as well: numerical modeling studies indicate that both the rate of global ocean overturning circulation and the meridional heat transport are sensitive to the value of K_v in the upper pycnocline (Bryan 1987).

The first step in the process of parameterizing mixing in terms of a diffusivity is to measure the mixing rate. This is not a simple task, owing partly to the small scales of mixing phenomena and partly to the intermittency of

mixing in space and time. Many techniques have been developed for measuring ocean mixing, techniques which may be divided broadly into “indirect” and “direct” categories. Indirect methods infer mixing rates from surrogate signals (e.g., shear) interpreted with the aid of theoretical models of the mixing process, for example, shear-driven turbulence versus double-diffusive mixing (Osborn and Cox 1972; Hamilton et al. 1993; McDougall and Ruddick 1992; Ruddick et al. 1997). Direct methods are based on observation of the results of mixing (e.g., spreading of injected dyes or tracers) and therefore require no assumptions about what causes the mixing.

The first inferences of mixing rates were made using naturally occurring tracers such as temperature. The classic example is Munk’s study of mixing in the North Pacific (Munk 1966). Assuming a steady-state heat balance between cooling by upwelling of cold water and warming by downward diffusion of warm surface water, he reasoned that

$$w \frac{\partial T}{\partial z} = K_v \frac{\partial^2 T}{\partial z^2}, \quad (1)$$

where w is the upward velocity, T is the temperature smoothed over large scales, and K_v is the vertical diffusivity appropriate to these scales, assumed to be depth-independent. In this way, Munk inferred a K_v of $1 \times 10^{-4} \text{ m}^2 \text{ s}^{-1}$, within a factor of 2 or so (see below).

Corresponding author address: Dan Kelley, Dept. of Oceanography, Dalhousie University, Halifax, NS B3H 4J1, Canada.
E-mail: Dan.Kelley@Dal.CA

In addition to studies based on the steady-state assumption, much has been learned from transient signals. The most direct studies involve releasing a quantity of an inert tracer into the ocean and monitoring its advection and diffusion. A key example is the North Atlantic Tracer Release Experiment (NATRE) study in the North Atlantic, in which SF_6 was injected on an isopycnal near 300-m depth and monitored for over a year (Ledwell et al. 1993, 1994). The spreading of the patch implied a vertical diffusivity of $1.1 \times 10^{-5} \text{ m}^2 \text{ s}^{-1}$ to $1.5 \times 10^{-5} \text{ m}^2 \text{ s}^{-1}$. The latter value is based on sampling in the spring season, and may be larger because winter mixing is more vigorous. This is consistent with the results of microstructure sampling in the region, $K_V = 1.0 \times 10^{-5} \text{ m}^2 \text{ s}^{-1}$ in autumn and $2.2 \times 10^{-5} \text{ m}^2 \text{ s}^{-1}$ in spring (Ruddick et al. 1997).

Tritium, released in the early 1960s during atmospheric bomb testing, has also been used as a tracer of ocean waters. Its spreading over the past three decades has provided valuable clues about ocean advection and mixing (e.g., Rooth and Östlund 1972; Michel and Suess 1975; Jenkins 1980; Fine et al. 1981; Jenkins 1988; Van Scoy et al. 1991a,b; Van Scoy and Druffel 1993).

The present study is based on a compilation of most known tritium measurements in the North Pacific. The dataset is concentrated in the central and eastern subtropical gyre and spans the three decades since the introduction of this tracer by bomb testing in the atmosphere. Our goal is to infer K_V from the observed spreading rate of the tracer.

It will be shown that the spatial density of sampling is insufficient to map variations in K_V horizontally. Therefore, to achieve statistical reliability, we will average zonally and meridionally within the subtropical gyre. Since the boundary of our averaging domain roughly corresponds to a streamline of the wind-driven circulation, the averaging process has the additional benefit of reducing the confounding effects of horizontal advection, as described in section 2. The tritium database is described in sections 3 and 4. The procedure for estimating K_V is described in section 5, along with the results. The paper ends with a summary in section 6.

2. Models of diffusion

Although the ocean advection–diffusion field is three-dimensional, it is not uncommon to use models with reduced dimensionality in order to simplify analysis. Such models have been highly successful in predicting ocean features that were later verified by more complex models. Prominent two-dimensional examples are depth-integrated streamfunction models of wind-driven circulation (e.g., Gill 1982) and zonally integrated models of overturning thermohaline circulation (Wright and Stocker 1991, 1992).

For a long time, one-dimensional models have been used in studies of pycnocline mixing, for example, the Munk analysis described in the last section. Munk noted

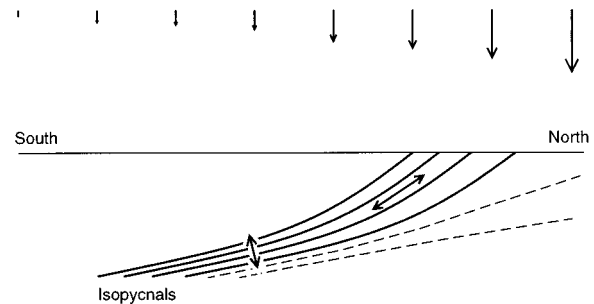


FIG. 1. Definition sketch illustrating how ventilation leads to a surface peak in tritium concentration at the northern edge of gyre (to right on diagram) and to a middepth peak in the gyre interior (to left on diagram). Arrows at top of diagram denote the atmospheric input function, which increases to the north (see Fig. 4). Drawn below the arrows is an ocean cross section showing outcropping isopycnals (bold lines) and nonoutcropping isopycnals (thinner, dashed, lines). Double-ended arrows indicate strong mixing along isopycnal surfaces and weaker mixing across isopycnals. The outcropping isopycnals act as a conduit through which the high levels of tritium in the northern regions may leak into (ventilate) the middepth waters of the central gyre.

that the diffusivity he calculated was about an order of magnitude higher than other estimates. Much has been made of this discrepancy in the years since, particularly relating to the effects of fluxes along isopycnal surfaces, pycnocline ventilation, and enhanced mixing near boundaries such as continental shelves and midocean ridges (see, e.g., Munk and Wunsch 1998).

One goal of the present paper is to perform an analysis that is reminiscent of Munk's, but using a transient tracer to avoid the necessity of estimating the upwelling rate. We will also lessen the constraint of his one-dimensional assumption, using something akin to the $1\frac{1}{2}$ scheme devised by Killworth and Smith (1984) in their study of mixing and ventilation in the Arctic pycnocline. Such $1\frac{1}{2}$ -dimensional schemes are designed to account partially for middepth renewal of fluid by lateral mixing and advection.

To establish notation, consider the idealized case of one-dimensional diffusion of a nondecaying tracer inserted instantaneously at time $t = 0$ in a vanishingly thin layer centered at depth $z = z_0$. (The assumption of instantaneous insertion in an infinitesimally thin layer greatly simplifies the analysis. The appendix illustrates that the assumption leads to errors that are small compared to the uncertainties stemming from the sparseness of the observations.) Attention is not restricted to the case of surface injection, $z_0 = 0$, because spreading from middepth mode waters is the likely route of injection into the midgyre waters (Fig. 1). Our analysis assumes diffusion within a semi-infinite domain, $-\infty < z < 0$, instead of the finite domain reaching to the ocean bottom; this assumption is valid until the tracer diffuses to the ocean bottom, which would take several thousand years given an ocean depth of 5 km and $K_V < 10^{-4} \text{ m}^2 \text{ s}^{-1}$.

If the column-integrated concentration is denoted

$F = \int_{-H}^0 C(z, t) dz$ and if mixing is described by depth-independent diffusivity K_v , with constant vertical velocity w , then the solution of the one-dimensional governing differential equation for tracer concentration

$$\frac{\partial C}{\partial t} = -w \frac{\partial C}{\partial z} + K_v \frac{\partial^2 C}{\partial z^2} \quad (2)$$

is a reflected-Gaussian profile whose peak thickens over time; that is,

$$C = \frac{1}{\sqrt{2\pi} D} \left\{ \exp \left[-\frac{1}{2} \frac{(z - z_0 + wt)^2}{D^2} \right] + \exp \left[-\frac{1}{2} \frac{(z + z_0 + wt)^2}{D^2} \right] \right\} \quad (3)$$

with $D = \sqrt{2K_v t}$ being the time-dependent thickness of the Gaussian peak. The second Gaussian term is required to yield $\partial C / \partial z = 0$ at $z = 0$, representing the vanishing of diffusive flux at the sea surface. This term is a ‘‘reflection’’ in the sense that the peak value of the term lies above the ocean surface, at equal distance from the surface as the peak in the water column. For $D^2/z_0^2 \ll 1$, this second term is negligible compared to the first term, throughout the water column. Such is the case in tracer-release experiments, where observations of tracer spreading are made before the tracer has had time to diffuse up to the surface. For this reason, tracer-release studies (e.g., Ledwell et al. 1993) employ a model of the above form without the second term. Here, both terms are needed since z_0 and D are comparable (see below).

The above equation provides a way to infer K_v from the rate of spreading of a tracer. Fitting individual profiles to the indicated functional form, without the wt term, yields values of D as a function of time, and from these the diffusivity can be estimated from

$$K_v = \frac{1}{2} \frac{\partial D^2}{\partial t}. \quad (4)$$

The upwelling rate w falls out of the analysis for K_v since it only determines the depth of the peak in tracer concentration, not the width of the peak. The time-dependent nature of this problem, arising because the tritium input was unsteady, releases us from the necessity of estimating w , as Munk (1966) had to do in his steady-state analysis of temperature profiles in the subtropical Pacific.

Three-dimensional advective–diffusive systems require the addition of horizontal advection and mixing terms to (2), and forcing a one-dimensional interpretation of such a system can lead to spurious effects. For example, consider the next simplest physical system, with the addition of horizontal advection but not horizontal diffusion, and focus on the signals associated with an isolated patch of tracer inserted at middepth at a given location. The patch will move with the horizontal flow

as it spreads vertically. For the case of closed streamlines, the patch will cycle endlessly, thickening vertically over time. Therefore, measurements made at a fixed location along the trajectory will reveal a precipitous thickening phase ($\partial D^2 / \partial t > 0$) as the patch approaches the measurement site, followed by a precipitous thinning phase as the patch passes by. A time series of $D(t)$ taken during the thickening phase could be misconstrued as indicating a large diffusivity, while a time series during the thinning phase would indicate spurious negative diffusion. The same would apply also in the case with horizontal diffusion, except that the spurious thickening/thinning signals would be less abrupt.

If $K_H = 0$, this spurious effect can be removed by integrating (averaging) the signals along the closed streamlines. In this way, the anomalous thickening on the upwind side of a patch cancels out the anomalous thinning on the downwind side. However, integration along streamlines will not remove the effect of advection if the tracer diffuses significantly from streamline to streamline. A measure of the rate of advection along streamlines, relative to diffusion across streamlines, is the nondimensional Peclet number, $Pe = UL/K_H$, where U is a scale value for horizontal velocity and L is a horizontal length scale of the flow (Musgrave 1990; Richards et al. 1995). For Sverdrup wind-driven flow, $U \sim 2 \times 10^{-2} \text{ m s}^{-1}$ (Gill 1982) and the north–south length-scale set by the wind stress curl is $L \sim 5 \times 10^6 \text{ m}$ (Levitus 1988) so that for $K_H \sim 10^3 \text{ m}^2 \text{ s}^{-1}$ (Sundermeyer and Price 1998) the Peclet number is of order 10^2 . To a first-order approximation, therefore, the system is predominantly advective, indicating that integrating within closed contours should reduce the temporal effects of advection without undue statistical bias of the signal by diffusion. A full accounting of all terms requires three-dimensional numerical modeling (e.g., Toggweiler et al. 1989), including proper simulation of seasonality in the ventilation process (Luyten et al. 1983; Woods 1985; Liu and Pedlosky 1994; Marshall and Marshall 1995). This is beyond the scope of the present paper.

The distribution of the closed streamlines of the time-averaged subtropical gyre is indicated by the density field of the upper ocean. Figure 2 shows the depth of the $1026.25 \text{ kg m}^{-3}$ potential density surface. This density value lies between the maximal wintertime surface outcropping density and the maximal density at 100-m depth, and is chosen to represent the maximal wintertime outcropping density of the wind-mixed surface layer of the subtropical gyre (recall Fig. 1). The depth contours define the bottom of the ‘‘bowl’’ of the ventilated wind-driven gyre, illustrating that the subtropical gyre extends from about 5°N to 40°N . It is within these limits, taken as bounding the closed streamlines of the subtropical gyre circulation, that the diffusive signal will be averaged in the present analysis.

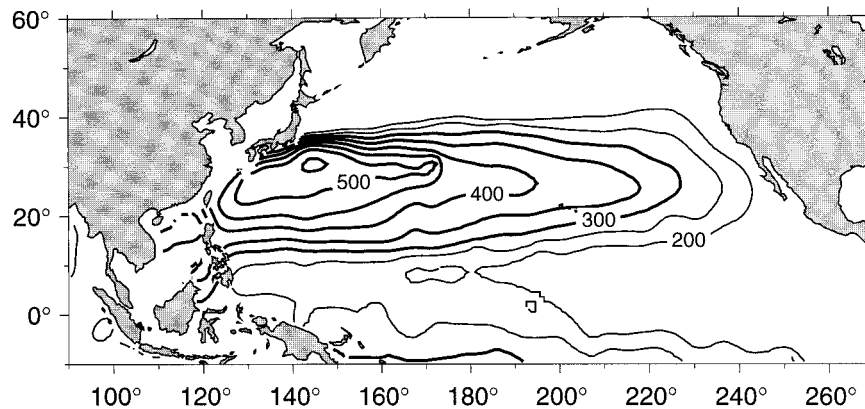


FIG. 2. Map of winter penetration depth, in meters, of the $\rho_0 = 1026.25 \text{ kg m}^{-3}$ isopycnal, an indication of the geometry of the "bowl" of the ventilated pycnocline. Thin contour lines indicate penetration depths of 200 m and 250 m; thicker lines indicate depths of 300 m, 350 m, etc. Data from Levitus and Boyer (1994).

3. Tritium source function

Tritium (^3H), the heaviest isotope of hydrogen, is produced naturally in the atmosphere at very low levels and is transferred to the ocean surface via precipitation and water vapor exchange. Nuclear weapons testing in the late 1950s and early 1960s resulted in large quantities of anthropogenic tritium being injected into the troposphere and stratosphere, predominately in the Northern Hemisphere. The yearly springtime breakup of the polar vortex supplied tritium to the high northern latitudes for several years after the bomb injection, giving tritium a special utility as a tracer of high Northern Hemisphere processes (see Weiss and Roether 1980).

Most of the anthropogenic tritium was delivered to the sea surface either directly, by vapor exchange and precipitation, or indirectly, as continental runoff in the form of ^3HHO . Once in the oceans, ^3HHO behaves in the same way as H_2O , with chemical fractionation effects being negligible (Suess 1969).

Tritium concentrations are expressed in tritium units (TU), where 1 TU equals a tritium/hydrogen abundance ratio of 10^{-18} . All tritium values presented here have been decay corrected to 1 January 1981 and are expressed in units TU81. The use of a common reference time for decay correction permits direct comparison between tritium concentrations measured at different times. This correction is based on the change of variable from $C(x, y, z, t)$, the concentration observed at time t , to $C_0(x, y, z, t_0)$, the concentration that would have been observed at a reference time t_0 . The change of variable is defined by the first-order tracer decay equation

$$C(x, y, z, t) = C_0(x, y, z, t_0)e^{-\lambda(t-t_0)}, \quad (5)$$

where $\lambda = 0.05576 \text{ yr}^{-1}$ is the first-order radioactive decay constant. This decay constant corresponds to the 12.43 yr half-life suggested by Unterweger et al. (1980). The value of the decay constant is implicit in reported tritium concentrations. The data used in this analysis

were measured using a slightly different estimate of the decay constant. Accordingly, we had to adjust the observed concentrations before applying the decay correction. We followed the scheme of Östlund and Rooth (1990), multiplying the concentrations by $1.0204 + (t - 1970) \times 8 \times 10^{-4}$, where t is in calendar years AD.

Decay correction transforms the governing equation for a decaying tracer,

$$\frac{\partial C}{\partial t} + \lambda C + \mathbf{u} \cdot \nabla C = K_H \nabla_H^2 C + K_V \frac{\partial^2 C}{\partial z^2}, \quad (6)$$

by removing the decay term (λC). The advantage is that decay-corrected tritium concentration obeys the same advection diffusion equation as nondecaying tracers.

The prebomb tritium values in the surface water of the North Atlantic were estimated to be 1 TU (uncorrected for radioactive decay) in 1953–54 (Giletti et al. 1958; Dreisigacker and Roether 1978). In an isolated system this would correspond to a decay-corrected value of 0.2 TU81. Therefore water containing less than 0.2 TU81 could theoretically reflect cosmogenic background tritium levels.

The input function has been mapped as a function of time and space through measurements of tritium concentration in precipitation and runoff. As a function of time the input was impulse-like, with tritium concentration in precipitation reaching a peak in 1963 (Fig. 3). The peak width, expressed as an e -folding scale or half-width, is 1 to 2 yr. (For more discussion of the temporal and spatial input function, see appendix.) The spatial variation of source function is mostly a function of latitude, with values increasing strongly from equator to pole (Fig. 4), consistent with the definition sketch of Fig. 1.

4. Tritium inventory

a. Data sources

We have compiled tritium measurements made in the North Pacific over several decades since the anthropo-

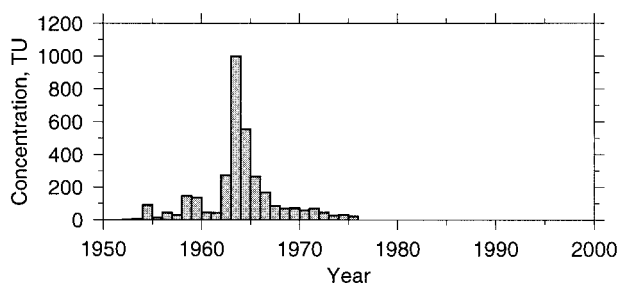


FIG. 3. History of tritium concentration in precipitation monitored at several stations at 50°N. Note peak of the input function in the early 1960s. Data from Weiss and Roether (1980).

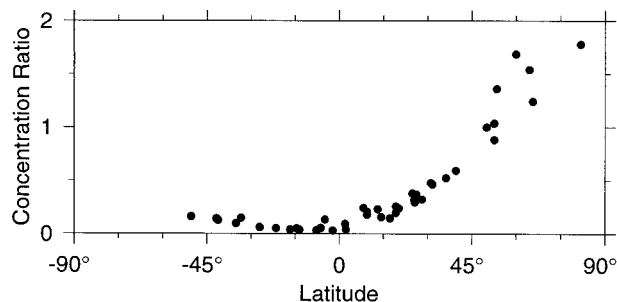


FIG. 4. Meridional variation of tritium input function, expressed as the ratio of precipitation tritium concentration as a function of latitude, divided by the concentration at 50°N. Note higher values at high latitudes. Data from Weiss and Roether (1980).

genic tritium production began. The data sources are summarized in Table 1, and a lengthy description of most of the data can be found in Van Scoy et al. (1991a) and Fine et al. (1981).

The measurement error for most of the post-1973 tritium measurements is taken to be 0.05 TU81 or 3.5%, whichever is larger (Östlund and Brescher 1982). Mea-

surement error for the earlier data tends to be somewhat larger.

b. Data sampling density

The sampling history is shown in Fig. 5. In total 369 stations are available, starting roughly in 1970, some 7

TABLE 1. Data sources.

Cruise	Time	Location	Source
Benthic 8	Apr–May 83	9°S–28°N along 123°W	Östlund et al. (1986)
EPOCS 2-80-OC	Mar–Apr 80	Three equatorial stns	Östlund et al. (1986)
EPOCS 3-80-RS	Jun–Jul 80	2°S–2°N at 95°W; 2°–3°N at 85°W	Östlund et al. (1986)
EPOCS 4-79	May–Jun 79	5°S–15°N along 110°W	Östlund et al. (1986)
GEOSECS	Aug–Sep 73; May–Jun 74	Geochem. Ocean Sections Study	Östlund and Brescher (1982)
GOGO 71	Nov 71	GEOSECS intercalibration stn.	Roether (1974)
Great Bear	May–Jun 70	Stns along 146°W	Miyake et al. (1975)
La Pared	Apr–May 65	Several subtropical stns	Michel (1974)
Marathon	May–Jun 84	Transect nominally along 152°W	Östlund (1987c)
Moana 85	Jul 85–Aug 85	Equatorial Pacific	Östlund (1996, personal communication)
Niiler 83	Jul 83	W. subtropical N. Pacific study	Östlund (1985a)
NOAA 81	Jul 81	Several subtropical stns	Östlund (1994, personal communication)
NOAA 82	May–Jun 82	Subtropical N. Pacific Study	Östlund (1984)
NOAA 83	Mar–Apr 83	24°–40°N along 170°W	Östlund (1985b)
NORPAX 1	Feb 79	4°–10°N along 153°W	Östlund et al. (1986)
NORPAX 3	Apr 79	1°N–6°N along 150°W	Östlund et al. (1986)
NORPAX 7	Sep 79	6°N, 156°30'W	Östlund et al. (1986)
NORPAX 9	Nov 79	3°S–20°N along 158°W	Östlund et al. (1986)
NORPAX 11	Jan 80	4°–10°N along 158°W	Östlund et al. (1986)
NORPAX 15	Jun 80	6°N, 158°W	Östlund et al. (1986)
Stn November	May 71–Nov 73	Time series at OWS N, 30°N, 140°W	Michel (1974)
Stn Papa 82	Jun 79–May 82	Time series at OWS P, 50°N, 145°W	Östlund (1985c)
Stn Papa 85	Apr 85	OWS P, 50°N, 145°W	Östlund (1986)
Stn Papa 93	Aug 93	OWS, P, 50°N, 145°W	Wong (1995, personal communication)
PEQUOD 81	Jan 81	2°S–12°N along 138°W	Östlund et al. (1986)
PEQUOD 82	Apr 82	2°S–12°N along 138°W	Östlund et al. (1986)
Phoenix	Dec 71–Feb 72	Several tropical stns	Miyake et al. (1975)
PRE-FGGE	Dec 77	2°S–20°N at 150°W	Östlund et al. (1986)
SagaII	Jun 87	Two stns from W. subpolar gyre	Östlund (1991)
Seventow	Feb–Jul 70	Stns throughout N. Pacific	Michel (1974)
Southerncross	Nov–Dec 68	Two tropical stns	Miyake et al. (1975)
Southtow	Jan–Sep 72	Eastern tropical Pacific	Michel (1974)
Styx	Aug 68	Central tropical Pacific	Michel (1974)
TPS 10	Feb–May 89	Transect nominally along 10°N	Jenkins (1994, personal communication)
TPS 24	Mar–May 85	Transect nominally along 24°N	Östlund (1987b)
TPS 47	Aug–Sep 85	Transect nominally along 47°N	Östlund (1987a)
WEPOCS 85	Jun–Jul 85	W. Eq. Pacific Ocean Circ. Study	Östlund (1994, personal communication)
WEPOCS 88	Jun–Jul 88	W. Eq. Pacific Ocean Circ. Study	Östlund (1990)

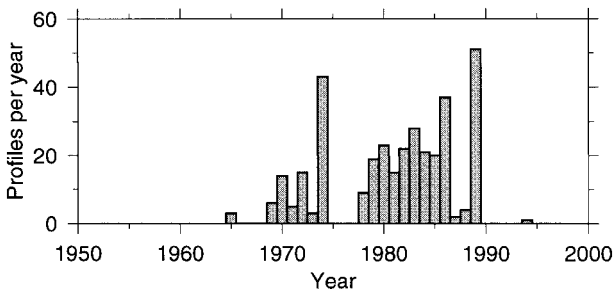


FIG. 5. Temporal distribution of tritium observations in North Pacific used in this study (see Table 1 for cruise names and data sources).

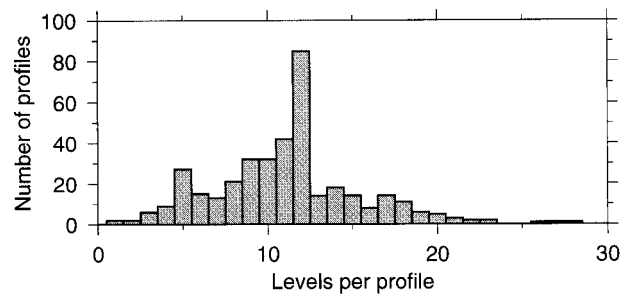


FIG. 6. Histogram of number of tritium levels per profile.

years after the peak of the source function (Fig. 3). The 10 year spanning the late 1970s to the late 1980s are the best sampled. The sampling rate seldom exceeds 50 profiles per year, being typically 10–20 profiles per year during the 1980s and half that in the 1970s. Sampling was concentrated in years of major expeditions, for example, the Geochemical Ocean Sections Study (GEO-SECS).

The number of tritium levels per profile ranged from 1 to just under 30, with a median of 11 (Fig. 6). Half of the profiles had between 8 and 13 levels and less than 5% of the profiles had fewer than 5 levels (a fact that will be used later, when it comes to fitting functions to the profiles).

Given approximately four hundred profiles in a domain that is 50° lat by 120° long, we have roughly 1 profile per a square 400 km wide (Fig. 7). Even with contemporaneous sampling, this spatial coverage could not possibly resolve eddies or boundary currents such as the Kuroshio. Indeed, coverage in the western third of the region is especially sparse (Fig. 8). The coverage is better in the central region, apart from a nearly 10-yr gap with no observations at any latitude. In the eastern region, the coverage is much denser, the main gap being an ~ 7 -yr gap in the latitude band making up the northern zone of the subtropical gyre (i.e., 20° – 40° N). This suggests that the present dataset is sufficient to resolve decadal variability of the subtropical gyre if one performs spatial averaging over a scale comparable to the gyre itself.

c. Data selection

Each tritium profile was fitted individually to the reflected-Gaussian profile of equation (3), without the w term. (Neglect of the w term does not yield incorrect results if $w \neq 0$. Rather, this simply means that no curve-fit is done for the value of w , a parameter not of primary interest here.) The parameters of the curve-fit were peak-depth z_0 , peak width D , and depth integral F . The curve-fit was done in a least squares manner, based on a cost-function defined as the squared deviation between the fit and the observed tritium values in the profile.

This function was minimized in (z_0, D, F) space using the Nelder–Mead simplex method (Press et al. 1995).

It was observed that not all of the profiles were able to statistically constrain the fit for these parameters. To begin with, since the model profile has three parameters (z_0 , D , and F) profiles with fewer than three levels are unable to provide adequate statistical constraint. To ensure at least two statistical degrees of freedom, we discarded profiles with fewer than five levels. This was not a particularly stringent criterion because most profiles had five or more levels (Fig. 6). However, visual inspection of each of the profiles and the corresponding curve-fits indicated that this criterion was not enough to obtain reliable results for all profiles. Therefore, we devised four additional requirements of profiles as follows.

- 1) Profiles with just one observation in the depth range of the fitted peak (i.e., in $z_0 - D < z < z_0 + D$) were discarded. This criterion, by itself, removed 3% of the profiles.

- 2) Profiles that matched poorly the presumed functional form were rejected using a goodness-of-fit test. We required that the ratio of the mean-squared deviation between the tritium concentration and the fitted value be < 0.4 times the mean-squared tritium concentration for the profile. This criterion, by itself, removed 1% of profiles.

- 3) Profiles leading to wildly extrapolated peaks in the fitted function were rejected. We required that the tritium value at the peak of the fitted function be no more than 10% in excess of the largest observed value. This criterion, by itself, eliminated 2% of the profiles.

- 4) Finally, profiles were rejected if they provided nonrobust statistical prediction of the D parameter. Robustness was determined by performing a Monte Carlo simulation in which each profile was repeatedly altered and then subjected to the curve-fitting procedure. In each repetition, the tritium value at each level was modified by the addition of random perturbations. These perturbations were chosen from a Gaussian statistical distribution with a mean of zero and a standard deviation equal to the tritium measurement uncertainty. This uncertainty was taken to be 3.5% for tritium values exceeding 0.7 TU81 and 0.05 TU81 otherwise, following (Östlund and Brescher 1982). A hundred trials were

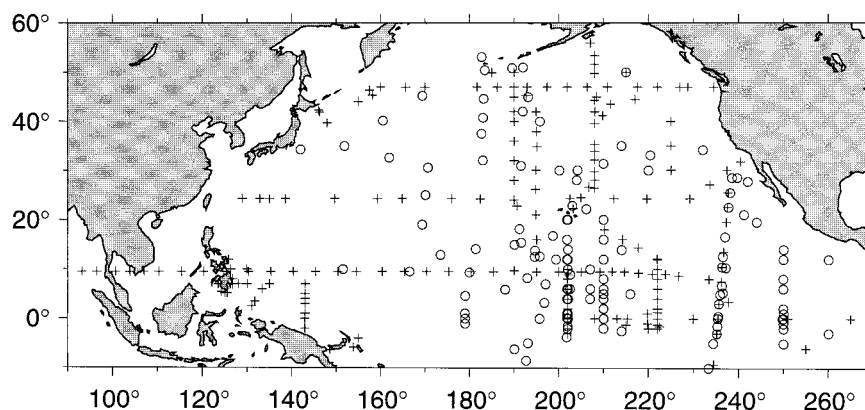


FIG. 7. Spatial distribution of tritium profiles. Circles and plus-signs indicate observations made before and after 1 January 1980, respectively.

done for each profile, and a histogram of the inferred D value was created. Profiles were rejected if the span between the third and first quartile of this histogram exceeded 0.75 times the median value. This scatter criterion, by itself, removed 8% of the profiles, some of which were also rejected by the previous criterion.

In all, these criteria led to the rejection of 13% of the observed profiles, leaving 318 profiles to be used in our analysis. The fit of the model profile to the observations was generally good, with the statistically unexplained variance being of order 1/10th of the observed variance (Fig. 9).

The subsequent analysis was based on the median value of D from the Monte Carlo procedure, with 100

repetitions, as applied to each profile in turn. This procedure yielded a dataset of the form $D = D(x, y, t)$, that is, each tritium profile was reduced to a single datum.

d. Spatial variation in tritium concentration

The overall variation of tritium concentration with depth can be described generally as a decrease from a range of 2 to 10 TU81 in the top kilometer to a range of 0 to 2 TU81 a kilometer below (Fig. 9). However there is substantial scatter in this distribution, with the standard deviation in any given depth range being comparable to the mean. This scatter results from the combination of profiles with widely ranging depth distributions (as a function of time and space), more than from scatter in individual profiles.

The profiles fall into two categories. In the first category, the maximum tritium concentrations are near the surface, as expected for diffusion from the surface downward (e.g., Fig. 10, left panel). Such profiles tend to be located in the subpolar gyre and near the northern edge of the subtropical gyre. In the second category, the tritium peak is at middepth (e.g., Fig. 10, right panel). These profiles are typically found in the central regions of the subtropical gyre. Thus, the variation in the type of vertical profile matches the expectation for a ventilated pycnocline (Fig. 1).

The general pattern is, as expected, with the depth of maximal tritium concentration roughly matching the base of the ventilated pycnocline (compare Figs. 11 and 2).

5. Calculation of diffusion rate

a. Inference based on decadal penetration

As a preliminary estimate of the effect of temporal variation, the observations made prior to 1 January 1980 were compared with the observations made after that time. In each time interval, the $D(x, y)$ values were cast onto a uniform latitude–longitude grid by using a two-

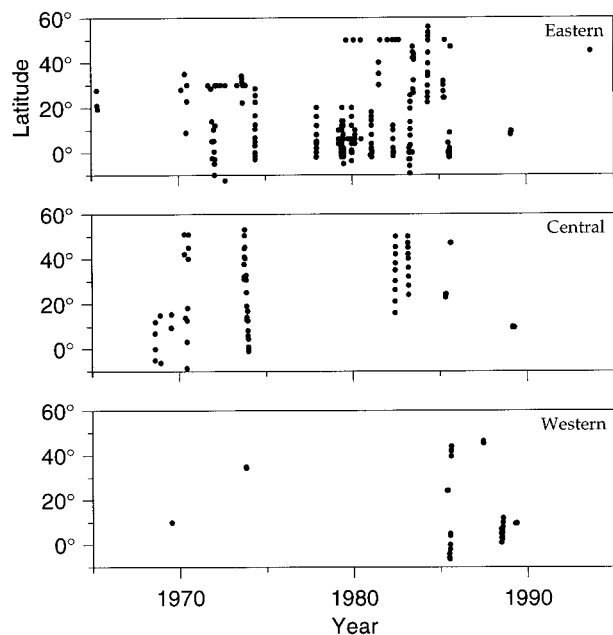


FIG. 8. Time–space distribution of tritium profiles. The panels indicate the latitude and time of profiles classified by longitude in three bands: “western,” to the west of 160°E; “central,” between 160°E and 200°E; and “eastern,” to the east of 200°E.

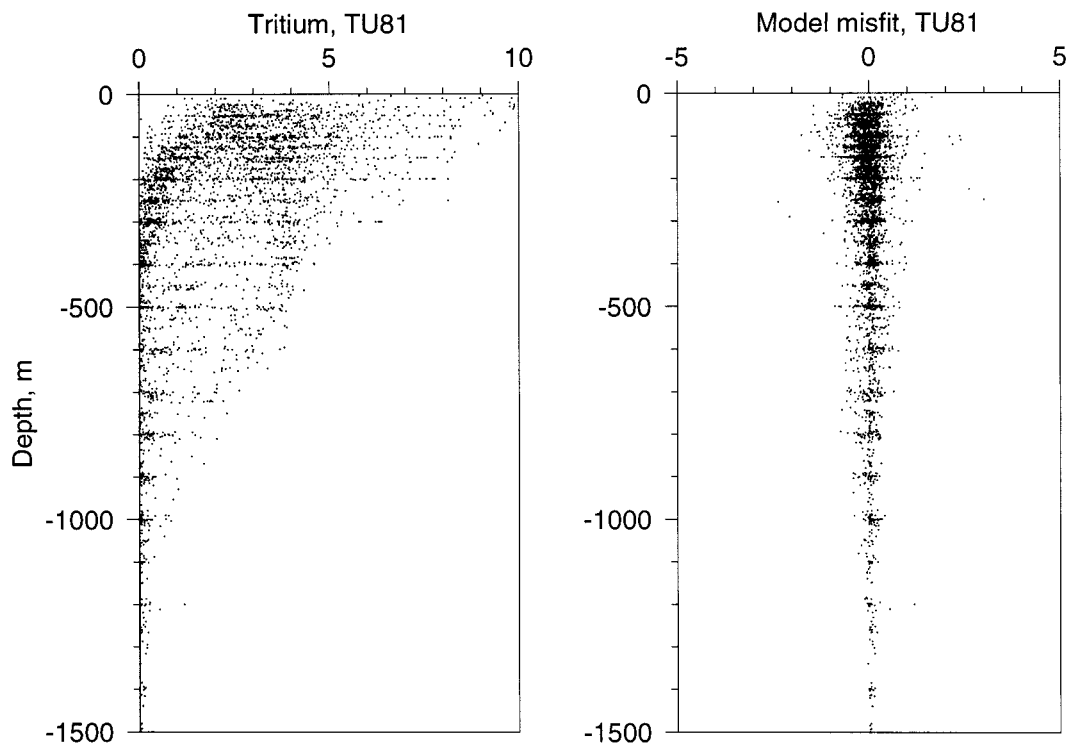


FIG. 9. (left) Variation of tritium concentration with depth, across whole time and space domain, for all profiles. (right) Difference between observed tritium values and the values predicted by the fitted profile according to Eq. (3).

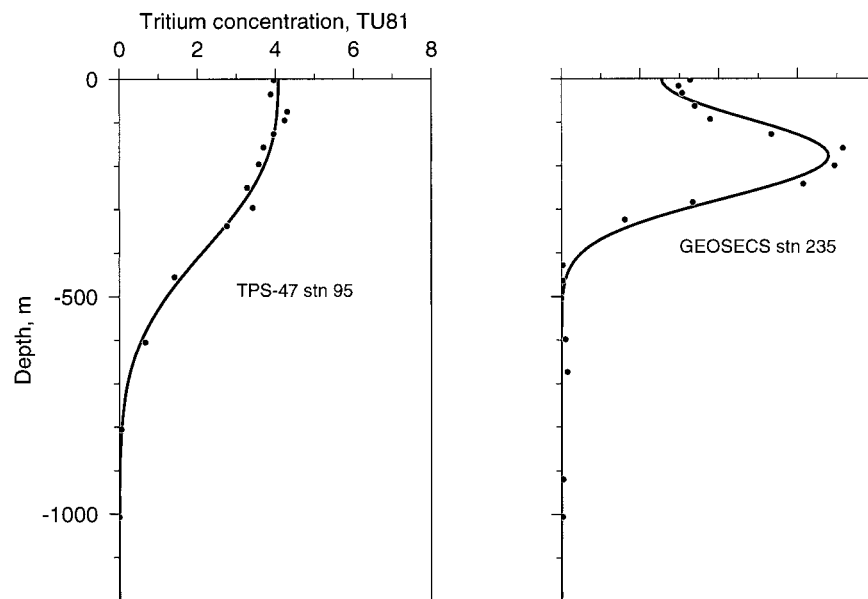


FIG. 10. Sample tritium profiles. (left) Typical profile in directly ventilated region at north of subtropical gyre: TPS-47 station 95 (year 1985.672, 47.0°N, 217.6°E). (right) Typical profile in midgyre, GEOSECS station 235 (year 1973.9, 16.8°N, 198.7°E). In each case the smooth curve represents the fitted profile.

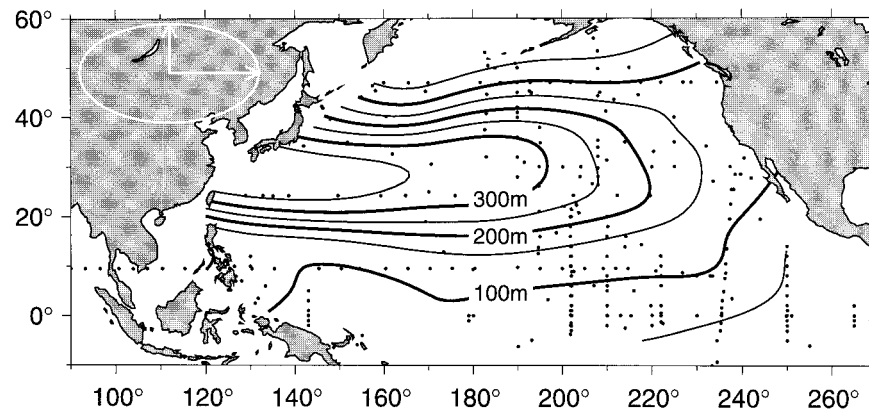


FIG. 11. Spatial variation of the depth, in meters, of the peak in the fitted tritium profiles. The gridding was done with the Barnes algorithm (see text) with initial meridional and zonal averaging radii indicated by the white ellipse drawn over Eurasia.

dimensional gridding procedure that is popular in the meteorological literature (Koch et al. 1983; Daley 1991; Barnes 1994). This so-called Barnes method is designed to capture large-scale variability in regions lacking densely spaced observations, and to capture smaller-scale variability in regions with denser sampling. The method is iterative. The first iteration corresponds to a moving-average filter on the observations. The filter shape is Gaussian, with possibly differing smoothing length scales in the x and y directions. Each succeeding iteration corresponds to a moving-average filter applied to the deviations between the observations and the gridded field as estimated during the previous iteration. It is common to employ successively smaller smoothing length scales in successive iterations. Based on the data spacing and on guidelines established by Koch et al. (1983), we chose to use two iterations, with initial smoothing length scales of 10° lat and 20° long. On the second iteration we divided these scales by $\sqrt{2}$.

For each of the two time periods, we computed a spatial average of this gridded field. Our intention in averaging the gridded field, rather than the raw data, was to remove the bias to be expected from differing latitude–longitude distribution of profiles in the two sampling periods.

The resultant spatial average of D in the 1970s was 162 m. The value raised to 191 m in the 1980s. From these two values, an estimate of K_V was made using (4) with a time interval of 10 yr. The result was $K_V = 1.7 \times 10^{-5} \text{ m}^2 \text{ s}^{-1}$, considering observations in both the subpolar and subtropical domains. A simple test of the sensitivity of this estimate to spatial variations in D was performed by restricting attention to selected geographical areas rather than the whole domain. For example, from observations in the central subtropical gyre (5° – 40° N, 160° – 240° E) we inferred the value $K_V = 1.2 \times 10^{-5} \text{ m}^2 \text{ s}^{-1}$. The difference between these estimates suggests that K_V may be inferred to no better than $\sim 30\%$. A similar factor arises from uncertainty in the

appropriate time interval to use in the first-difference approximation of $\partial D^2/\partial t$. The assumed interval of 10 yr between the 1970s average and the 1980s average may be uncertain to a factor of 50%, given that the 1980s data are spread throughout that decade (Fig. 5). These results suggest that the uncertainty in diffusivity might up to 50%, leading to an initial estimate of $K_V = (1.4 \pm 0.7) \times 10^{-5} \text{ m}^2 \text{ s}^{-1}$ for the subtropical gyre.

b. Inference based on gridding in time and space

The difficulty of comparing two decadal averaged D fields may be side-stepped by treating the time of observation as an independent variable just like latitude and longitude—that is, by applying a three-dimensional gridding technique based on a two-dimensional gridding technique described above, smoothing in time as well as space. Since the temporal smoothing interval should be a decade or less to measure variation over the decadal scale of the observations, it is necessary to increase spatial smoothing intervals, compared to those in the last section, to smooth over data gaps. Accordingly, we used spatial smoothing scales that were double those used in the last section. We also repeated the choice of two iterations and of reducing the scales by $\sqrt{2}$ in the second iteration.

The temporal smoothing scale was chosen based on the gaps in the observations. These gaps are of order a year at best and nearly a decade at worst (e.g., in the domain labeled “central” in Fig. 8). To cover the gaps, a smoothing radius of 7 yr was used, with sensitivity tests also being done with timescales of 5 yr and 10 yr, to provide error estimates for K_V .

We found that lack of data prevented robust inference temporal variation in D to the west of 160° E (Fig. 8). Therefore we concentrated on the central and eastern subtropical gyre (5° – 40° N, 160° – 240° E). We selected the $D(x, y)$ maps for the years 1975 and 1985, computing the average D value in the indicated spatial domain,

squaring this, then first-differencing over the 10 yr interval to calculate K_V according to (4). As a sensitivity test, this was done using a variety of smoothing timescales.

Diffusivities of value $1.0 \times 10^{-5} \text{ m}^2 \text{ s}^{-1}$ and $2.3 \times 10^{-5} \text{ m}^2 \text{ s}^{-1}$ result from using timescales of 10 yr and 5 yr, respectively. The shorter timescale is arguably too short to span the data void, implying that the larger value of K_V may be spurious. Conversely, the longer timescale had the effect of smoothing the time variation unduly so that the lower diffusivity is also somewhat suspect. However, these smoothing timescales may represent reasonable limits, so the corresponding diffusivities may also represent reasonable limits. An intermediate timescale of 7 yr results in a diffusivity of $1.6 \times 10^{-5} \text{ m}^2 \text{ s}^{-1}$. In summary, then, this method yielded $K_V = (1.6 \pm 0.7) \times 10^{-5} \text{ m}^2 \text{ s}^{-1}$ in the subtropical gyre.

c. Inference based on a least squares model

The gridding calculation has the advantage that bias due to spatial sampling is reduced. The disadvantage is that error bars are difficult to determine. Therefore, a third method was employed. In it, a least squares curve fit to model:

$$D = A_0 + A_1x + A_2y + A_3t \quad (7)$$

was fit to the data, where x is latitude, y longitude, and t time. Then $\partial D^2/\partial t$ was calculated as $\frac{1}{2}D\partial D/\partial t$, with $\partial D/\partial t$ given by the fitted model parameter A_3 and with D given by the mean over the domain. Error estimates in A_3 yield error estimates in K_V .

Restricting attention to the observations within the subtropical gyre ($5^\circ\text{--}40^\circ\text{N}$, $160^\circ\text{--}240^\circ\text{E}$) the correlation coefficient was found to be significant ($R^2 = 0.75$). The inferred diffusivity for the subtropical gyre was found to be $K_V = (1.5 \pm 0.6) \times 10^{-5} \text{ m}^2 \text{ s}^{-1}$.

6. Summary and conclusions

Tritium observations in the North Pacific, spanning three decades, were compiled and decay corrected to a common reference time. Generally, the depth dependence at any given location is described well by a reflected-Gaussian function of depth (3), as would be expected both for regions where tritium was added directly to the surface and for regions where it was added via subduction along isopycnals outcropping in the subpolar region. In agreement with previous studies of ventilation and mode waters, the peak of this reflected-Gaussian was found to lie near the surface at the northern edge of the subtropical gyre, and at a depth of about 300 m within the midlatitude gyre interior. The horizontal variation of the base-depth of the ventilated pycnocline corresponded well with that of the depth z_0 of the peak tritium value. This confirms that the midlatitude ocean takes up tritium (and, presumably, other substances) not only by direct mixing downward from the surface, but

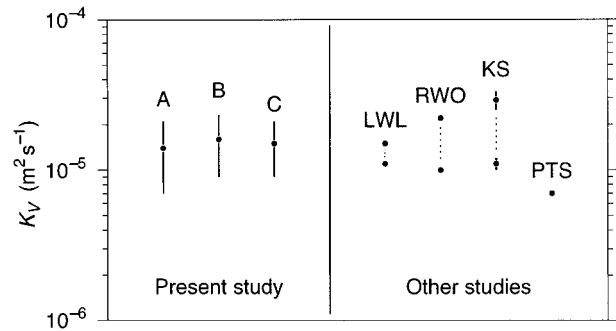


FIG. 12. Summary of inferred diffusivities from this and other studies. Case A: result from first-difference of maps of tritium peak-width (D) for observations before and after the year 1980. Case B: result from first-difference of time-varying fields formed by gridding D as a function of time as well as space. Case C: result from least-squares fit of D as a linear function of latitude, longitude, and time. Case LWL: result from NATRE tracer-release spreading rate (Ledwell et al. 1993). Case RWO: corresponding values inferred from NATRE microstructure observations (Ruddick et al. 1997). Case KS: result from a model of internal-wave mixing, using fincalse shear in Sargasso Sea, with values over convex and concave topography being shown in the upper and lower groups, respectively (Kunze and Sanford 1996). Case PTS: result from internal-wave mixing model, assuming the waves to be distributed according to a Garrett-Munk spectrum (Polzin et al. 1995).

also, and perhaps predominantly, by ventilation along the isopycnal surfaces at the base of the anticyclonic wind-driven gyres.

The parameter of most interest for the present study is the width, D , of the peak in the tritium profile since the temporal increase of this parameter is linked to the vertical diffusivity by $K_V = \frac{1}{2}\partial D^2/\partial t$.

Three techniques were used to infer the rate of change of D and thus K_V . In the first, the $D(x, y, t)$ values were divided into groups before and after 1 January 1980. Each $D(x, y)$ field was gridded in (x, y) and then averaged through the subtropical gyre. Then $\partial D^2/\partial t$ was calculated by first-difference. The result was $K_V = (1.4 \pm 0.7) \times 10^{-5} \text{ m}^2 \text{ s}^{-1}$. A weakness of this technique arises from the division of observations into just two time categories. We addressed this weakness in our second technique, based on gridding D through time and space together. The result, $K_V = (1.6 \pm 0.7) \times 10^{-5} \text{ m}^2 \text{ s}^{-1}$, agreed well with the first estimate. A third technique based on least squares regression instead of gridding also yielded similar results, $K_V = (1.5 \pm 0.6) \times 10^{-5} \text{ m}^2 \text{ s}^{-1}$. The correspondence of the estimates from the three techniques suggests that our results are robust.

In conclusion, our analysis of the rate of spreading of bomb tritium indicates that the basin-wide diffusivity in the surface half-kilometer of the central North Pacific subtropical pycnocline is $K_V = (1.5 \pm 0.7) \times 10^{-5} \text{ m}^2 \text{ s}^{-1}$. The value agrees well with inferences from other studies of mixing in the subtropical oceans (see summary in Fig. 12). In particular, our estimate of K_V for the North Pacific subtropical pycnocline matches the value obtained in the NATRE experiment in the North

Atlantic, suggesting a universal value for vertical diffusivity in such domains.

Acknowledgments. We thank the anonymous reviewers and the editor, Nelson Hogg, for helpful and insightful comments on the work. We also thank Eric Kunze, Brian May, and Scott Doney for comments on an earlier draft. Our work could not have been undertaken without the help of the many PIs who kindly made their tritium data available to us. In particular, we take pleasure in acknowledging the generosity of H. Göte Östlund. A glance at Table 1 will reveal that he contributed most of the data we used. Without him, our analysis would be impossible. DEK acknowledges support from an NSERC operating grant, and KVS acknowledges support from NSF Grant OCE-952960.

APPENDIX A

Validity of Assumed Impulsive Tritium Source

a. Introduction

The model tritium profile used in the text to infer K_v was based upon the assumption of a tritium source function that was impulsive in space and time, that is, instantaneous and limited to an infinitesimally thin depth interval. As discussed in the text, the model profile fits the observations well. Here we demonstrate the validity of the assumption of an impulsive source. For simplicity, we consider temporal and spatial diffusive effects separately in the sections below.

b. Nonimpulsive spatial source

A tracer with concentration $C = C(z, t)$ that is subject to constant diffusivity K_v in the domain $-\infty < z < \infty$ obeys

$$\frac{\partial C}{\partial t} = K_v \frac{\partial^2 C}{\partial z^2}. \quad (\text{A1})$$

If the initial profile is given by $C(z, 0) = \phi(z)$, the solution for later times is

$$C(z, t) = \frac{1}{\sqrt{4\pi K_v t}} \int_{-\infty}^{\infty} \phi(z') \exp\left[-\frac{(z-z')^2}{4K_v t}\right] dz' \quad (\text{A2})$$

(see, e.g., Carslaw 1921, §16).

This integral may be evaluated analytically for various simple forms of the initial condition $\phi(z)$. To address the sensitivity of our results, consider two initial conditions that form limiting cases.

First, consider an impulsive source, that is, a quantity F of tracer inserted at $t = 0$ into an infinitesimally narrow zone near $z = 0$. This implies $\phi(z) = F\delta(z)$ where $\delta(z)$ is the Dirac delta function. The solution to this “impulse” (subscript I) case is

$$C_I(z, t) = \frac{F}{\sqrt{4\pi K_v t}} \exp\left(-\frac{z^2}{4K_v t}\right). \quad (\text{A3})$$

As expected, this is a derivation of (3) in the text, for $z_0 = 0$ and $w = 0$ and with F adjusted to account for the infinite, as opposed to semi-infinite, domain.

Second, consider the case of the same amount of tracer inserted uniformly in a layer of finite thickness $2a$ centered at $z = 0$ so that the initial condition is described by a “top-hat” function; that is,

$$\phi(z) = \begin{cases} \frac{F}{2a}, & -a < z < a \\ 0, & \text{otherwise.} \end{cases} \quad (\text{A4a})$$

$$\quad (\text{A4b})$$

The solution to this top-hat (subscript T) case is

$$C_T(z, t) = \frac{F}{4a} \left[\operatorname{erf}\left(\frac{z-a}{\sqrt{4K_v t}}\right) + \operatorname{erf}\left(\frac{z+a}{\sqrt{4K_v t}}\right) \right] \quad (\text{A5})$$

in terms of the error function defined by

$$\operatorname{erf}(x) = \frac{2}{\sqrt{\pi}} \int_0^x e^{-s^2} ds \quad (\text{A6})$$

(see, e.g., Abramowitz and Stegun 1972).

After a sufficient long time interval, that is, for $t \gg a^2/K_v$, the solutions C_I and C_T converge. A rough calculation suggests that the convergence timescale is just a few years, given scale values $a^2 \sim 10^3 \text{ m}^2$ and $K_v \sim 10^{-5} \text{ m}^2 \text{ s}^{-1}$. To be more precise, we measured the rms deviation between C_I and C_T over the range $-500 \text{ m} < z < 0 \text{ m}$, given $K_v = 1.5 \times 10^{-5} \text{ m}^2 \text{ s}^{-1}$ and $a = 50 \text{ m}$. Indeed, the rms deviation drops rapidly with elapsed time, from 5% at 4 yr to <2% after 10 yr.

Since most of the tritium measurements were made more than a decade after the peak of the tritium source function, this suggests that only minimal errors should result from the assumption of an impulsive spatial input. This justifies the use of the model profile (3) used in the text to infer the diffusivity from the rate of tritium spreading. One might also note an additional advantage: assuming the spatial input was impulsive avoids the requirement of fitting for an additional model parameter (the insertion thickness, a).

c. Nonimpulsive temporal source

Turning now to the temporal source, consider (A1) with initial condition $C(z, 0) = 0$, but with time-dependent forcing at the boundary ($z = 0$). Given the input of tritium through precipitation and vapor exchange, the most appropriate boundary condition is expressed in terms of a time series of flux at the surface, instead of concentration there. Therefore we take the boundary condition to be in the form of a prescribed flux $\phi(t)$ (units TU m s^{-1}). Continuity of flux across the boundary implies

$$K_v \frac{\partial C(0, t)}{\partial z} = \phi(t). \quad (\text{A7})$$

Our task, then, is to examine the solution to (A1) given (A7) for various forms of $\phi(t)$. The solution given this type of forcing is most easily obtained after transformation to a gradient variable,

$$\theta = \frac{\partial C}{\partial z}, \quad (\text{A8})$$

which obeys

$$\frac{\partial \theta}{\partial t} = K_v \frac{\partial^2 \theta}{\partial z^2} \quad (\text{A9})$$

with initial condition $\theta(z, 0) = 0$ and boundary condition $\theta(0, t) = \phi(t)/K_v$. The transformation to θ has thus

transformed the boundary condition into a simpler form that has been studied exhaustively in problems of heat conduction in solids (see, e.g., Carslaw 1921, §9). The solution with this time-dependent boundary condition is

$$\theta = \frac{1}{K_v} \int_0^t \phi(\lambda) \frac{\partial F(z, t - \lambda)}{\partial t} d\lambda, \quad (\text{A10})$$

where $F(z, t)$ satisfies the same differential equation but with the steady boundary condition $F(0, t) = 1$. This yields

$$F = 1 - \operatorname{erf}\left(\frac{z}{\sqrt{4K_v t}}\right). \quad (\text{A11})$$

Differentiating (A11), substituting into (A10), integrating once to get $\theta(z, t)$ and a second time to get $C(z, t)$, yields the solution

$$C(z, t) = \frac{\Phi}{K_v} \left\{ z \operatorname{erf}\left(\frac{z}{\sqrt{4K_v(t-\tau)}}\right) - z \operatorname{erf}\left(\frac{z}{\sqrt{4K_v t}}\right) + \sqrt{\frac{4K_v(t-\tau)}{\pi}} \exp\left[-\frac{z^2}{4K_v(t-\tau)}\right] - \sqrt{\frac{4K_v t}{\pi}} \exp\left[-\frac{z^2}{4K_v t}\right] \right\}. \quad (\text{A12})$$

Equation (A12) provides the means to test the sensitivity of the diffusivity calculation used in the text. Our approach was to use (A12) to generate simulated profiles $C(z; t, \tau)$ at various times t , given application of tritium flux for various prescribed periods, τ . The resulting profiles were then analyzed as in the text, to determine the thickness D^* of the concentration peak, and thence the “observed” diffusivity, given by $K_v^* = \frac{1}{2} d(D^*)^2/dt$. Each simulation used $K_v = 1.5 \times 10^{-5} \text{ m}^2 \text{ s}^{-1}$. The test procedure relied on comparing the inferred diffusivity K_v^* to this supplied value, for a range of values of τ . For each τ value, 25 simulated profiles were generated at yearly intervals, starting one year after the end of the input (i.e., starting at $t = \tau + 1 \text{ yr}$).

As expected, small values of τ led to inferred diffusivities K_v^* that closely match the supplied value, with $K_v^* \rightarrow K_v$ as $\tau \rightarrow 0$. The computed error in diffusivity was $<6\%$ for $\tau < 10 \text{ yr}$, an interval significantly larger than the duration of the atmospheric concentration peak (Fig. 3) and $<1\%$ for $\tau < 3 \text{ yr}$, an interval arguably more representative of the atmospheric time series. Thus, the test suggests that the diffusivity inferred in the text is unlikely to suffer errors from the assumption of an impulsive temporal source of tritium.

REFERENCES

- Abramowitz, M., and I. A. Stegun, 1972: *Handbook of Mathematical Functions*, Dover, 1046 pp.
 Barnes, S. L., 1994: Application of Barnes objective analysis scheme.

- Part I: Effects of undersampling, wave position, and station randomness. *J. Atmos. Oceanic Technol.*, **11**, 109–116.
 Bryan, F., 1987: Parameter sensitivity of primitive equation ocean general circulation models. *J. Phys. Oceanogr.*, **17**, 970–985.
 Carslaw, H. S., 1921: *Introduction to the Mathematical Theory of the Conduction of Heat in Solids*. Macmillan, 268 pp.
 Daley, R., 1991: *Atmospheric Data Analysis*. Cambridge Press, 457 pp.
 Dreisigacker, E., and W. Roether, 1978: Tritium and ^{90}Sr in North Atlantic surface water. *Earth Planet. Sci.*, **38**, 301–312.
 Fine, R. A., J. L. Reid, and H. G. Östlund, 1981: Circulation of tritium in the Pacific Ocean. *J. Phys. Oceanogr.*, **11**, 3–14.
 Giletti, B. J., F. Bazan, and J. L. Kulp, 1958: The geochemistry of tritium. *Eos, Trans. Amer. Geophys. Union*, **39**, 807–817.
 Gill, A. E., 1982: *Atmosphere–Ocean Dynamics*. Academic Press, 662 pp.
 Hamilton, J. M., N. S. Oakey, and D. E. Kelley, 1993: Salt-finger signatures in microstructure measurements. *J. Geophys. Res.*, **98**, 2453–2460.
 Jenkins, W. J., 1980: Tritium and ^3He in the Sargasso Sea. *J. Mar. Res.*, **38**, 533–569.
 ———, 1988: The use of anthropogenic tritium and helium-3 to study subtropical gyre ventilation and circulation. *Philos. Trans. Roy. Soc. London A*, **325**, 43–61.
 Killworth, P. D., and J. M. Smith, 1984: A one-and-a-half dimensional model for the arctic halocline. *Deep-Sea Res.*, **31**, 271–293.
 Koch, S. E., M. DesJardins, and P. J. Kocin, 1983: An interactive Barnes objective map analysis scheme for use with satellite and conventional data. *J. Climate Appl. Meteor.*, **22**, 1487–1503.
 Kunze, E. L., and T. B. Sanford, 1996: Abyssal mixing: Where it is not. *J. Phys. Oceanogr.*, **26**, 2286–2296.
 Ledwell, J. R., A. J. Watson, and C. S. Law, 1993: Evidence for slow mixing across the pycnocline from an open ocean tracer release experiment. *Nature*, **364**, 701–703.
 ———, ———, and ———, 1994: Tracer dispersion during the North Atlantic Tracer Release Experiment (NATRE). *Eos, Trans. Amer. Geophys. Union*, **75**, 121.

- Levitus, S., 1988: Ekman volume fluxes for the world ocean and individual ocean basins. *J. Phys. Oceanogr.*, **18**, 271–279.
- , and T. P. Boyer, 1994: *World Ocean Atlas 1994*. NOAA Atlas NESDIS 4, U.S. Dept. of Commerce, 117 pp.
- Liu, Z., and J. Pedlosky, 1994: Thermocline forced by annual and decadal surface temperature variation. *J. Phys. Oceanogr.*, **24**, 587–608.
- Luyten, J. R., J. Pedlosky, and H. Stommel, 1983: The ventilated thermocline. *J. Phys. Oceanogr.*, **13**, 292–309.
- Marshall, D., and J. Marshall, 1995: On the thermodynamics of subduction. *J. Phys. Oceanogr.*, **25**, 138–151.
- McCartney, M. S., 1982: The subtropical recirculation of mode waters. *Deep-Sea Res.*, **40**, 427–464.
- McDougall, T. J., and B. R. Ruddick, 1992: The use of ocean microstructure to quantify both turbulent mixing and salt-fingering. *Deep-Sea Res.*, **39**, 1931–1952.
- Michel, R. L., 1974: Uptake of bomb-produced tritium by the Pacific Ocean. Ph.D. thesis, University of California, San Diego, 222 pp. [Available from UMI Dissertation Service, 300 N. Zeeb Rd., P.O. Box 1346, Ann Arbor, MI 48106-1346.]
- , and H. E. Suess, 1975: Bomb tritium in the Pacific Ocean. *J. Geophys. Res.*, **80**, 4139–4152.
- Miyake, Y., T. Shimada, Y. Sugimura, K. Shigehara, and K. Saruhasi, 1975: Distribution of Tritium in the Pacific Ocean. *Rec. Oceanogr. Works Japan*, **13**, 17–31.
- Munk, W. H., 1966: Abyssal recipes. *Deep-Sea Res.*, **13**, 707–730.
- , and C. Wunsch, 1998: Abyssal recipes II: Energetics of tidal and wind mixing. *Deep-Sea Res.*, **45**, 1977–2010.
- Musgrave, D. L., 1990: Numerical studies of tritium and helium-3 in the thermocline. *J. Phys. Oceanogr.*, **20**, 344–373.
- Osborn, T. R., and C. S. Cox, 1972: Oceanic finestructure. *Geophys. Fluid Dyn.*, **3**, 321–345.
- Östlund, H. G., 1984: TTO/North Pacific study, Discoverer 1982—Tritium results: Data release 84-10. University of Miami Tritium Laboratory, Miami, FL.
- , 1985a: Niiler cruise 1983 R/V *Thomas Thompson* 173 tritium samples: Data release 85-44 (amended in 86-22). University of Miami Tritium Laboratory, Miami, FL.
- , 1985b: TTO/North Pacific study, Discoverer 1983—Tritium results: Data release 85-37. University of Miami Tritium Laboratory, Miami, FL.
- , 1985c: Ocean station Papa tritium results 1979–1982: Data release 85-06. University of Miami Tritium Laboratory, Miami, FL.
- , 1986: Ocean Station Papa summer 1985 tritium and radiocarbon results: Data release 86-24. University of Miami Tritium Laboratory, Miami, FL.
- , 1987a: TPS47-transpacific cruise 1985 tritium results: Data release 87-33. University of Miami Tritium Laboratory, Miami, FL.
- , 1987b: TPS24-transpacific cruise 1985 tritium results: Data release 87-35. University of Miami Tritium Laboratory, Miami, FL.
- , 1987c: Marathon II North Pacific cruise R/V *Thomas Thompson* 1984 tritium results: Data release 87-20. University of Miami Tritium Laboratory, Miami, FL.
- , 1990: WEPOCS 3, 1988 tritium results: Data release 90-25. University of Miami Tritium Laboratory, Miami, FL.
- , 1991: SAGA-II cruise 1987 tritium results: Data release 91-05. University of Miami Tritium Laboratory, Miami, FL.
- , and R. Brescher, 1982: GEOSECS tritium, Data report No. 12. University of Miami Tritium Laboratory, Miami, FL.
- , and C. G. H. Rooth, 1990: The North Atlantic tritium and radiocarbon transients 1972–1983. *J. Geophys. Res.*, **95**, 20 147–20 165.
- , C. Grall, and R. E. Brescher, 1986: Equatorial Pacific tritium. Data report No. 15. University of Miami Tritium Laboratory, Miami, FL.
- Polzin, K. L., J. M. Toole, and R. W. Schmitt, 1995: Finescale parameterizations of turbulent dissipation. *J. Phys. Oceanogr.*, **25**, 306–328.
- Press, W. H., S. A. Teukolsky, W. T. Vetterling, and B. P. Flannery, 1995: *Numerical Recipes in C, the Art of Scientific Computing*. Cambridge University Press, 994 pp.
- Richards, K. J., Y. Jia, and C. F. Rogers, 1995: Dispersion of tracers by ocean gyres. *J. Phys. Oceanogr.*, **25**, 873–887.
- Roether, W., 1974: The tritium and carbon-14 profiles at the GEOSECS I (1969) and GOGO I (1971) North Pacific Stations. *Earth Planet. Sci.*, **23**, 108–115.
- Rooth, C. G., and H. G. Östlund, 1972: Penetration of tritium into the Atlantic thermocline. *Deep-Sea Res.*, **19**, 481–492.
- Ruddick, B., D. Walsh, and N. Oakey, 1997: Variations in apparent mixing efficiency in the North Atlantic Central Water. *J. Phys. Oceanogr.*, **27**, 2589–2605.
- Suess, H. E., 1969: Tritium geophysics as an international research project. *Science*, **163**, 1405–1410.
- Sundermeyer, M. A., and J. F. Price, 1998: Lateral mixing in the North Atlantic Tracer Release Experiment: Observations and numerical simulations of Lagrangian particles and passive tracer. *J. Geophys. Res.*, **103**, 21 481–21 497.
- Talley, L. D., 1985: Ventilation of the subtropical North Pacific: The shallow salinity minimum. *J. Phys. Oceanogr.*, **15**, 633–649.
- Toggweiler, J. R., K. Dixon, and K. Bryan, 1989: Simulations of radiocarbon in a coarse-resolution World Ocean model. Part II: Distributions of bomb-produced carbon 14. *J. Geophys. Res.*, **95**, 8232–8264.
- Unterwiesing, M. P., B. M. Coursey, F. J. Schima, and W. B. Mann, 1980: Preparation and calibration of the 1978 National Bureau of Standards tritiated-water standards. *Int. J. Appl. Rad. Isotopes*, **31**, 611–614.
- Van Scoy, K. A., and E. R. M. Druffel, 1993: Ventilation and transport of thermocline and intermediate waters in the North Pacific during recent El Niños. *J. Geophys. Res.*, **98**, 18 083–18 088.
- , R. A. Fine, and H. G. Östlund, 1991a: Two decades of mixing tritium into the North Pacific Ocean. *Deep-Sea Res.*, **38**, S191–S219.
- , D. B. Olson, and R. A. Fine, 1991b: Ventilation of North Pacific intermediate water: The role of the Alaskan gyre. *J. Geophys. Res.*, **96**, 16 801–16 810.
- Weiss, W., and W. Roether, 1980: The rates of tritium input to the world oceans. *Earth Planet. Sci.*, **49**, 435–446.
- Woods, J. D., 1985: The physics of thermocline ventilation. *Coupled Ocean-Atmosphere Models*. J. C. J. Nihoul and B. M. Jamart, Eds. Elsevier, 543–590.
- , and W. Barkmann, 1986: A Lagrangian mixed layer model of Atlantic 18°C water formation. *Nature*, **319**, 574–576.
- Wright, D. G., and T. F. Stocker, 1991: A zonally averaged ocean model for the thermohaline circulation. Part I: Model development and flow dynamics. *J. Phys. Oceanogr.*, **21**, 1713–1724.
- , and —, 1992: Sensitivities of a zonally averaged global ocean circulation model. *J. Geophys. Res.*, **97**, 12 707–12 730.